Available online at www.sciencedirect.com
SCIENCE DIRECT®
PERGAMON
International Journal of Heat and Mass Transfer 46 (2003) 2135–2148
International Journal of HEAT and MASS TRANSFER
www.elsevier.com/locate/ijhmt

An analytical solution for two-dimensional inverse heat conduction problems using Laplace transform

Masanori Monde *, Hirofumi Arima, Wei Liu, Yuhichi Mitutake, Jaffar A. Hammad

Department of Mechanical Engineering, Saga University, Honjo-machi 1, Saga-shi 840-8502, Japan

Received 28 June 2002; received in revised form 25 November 2002

Abstract

An analytical method has been developed for two-dimensional inverse heat conduction problems by using the Laplace transform technique. The inverse solutions are obtained under two simple boundary conditions in a finite rectangular body, with one and two unknowns, respectively. The method first approximates the temperature changes measured in the body with a half polynomial power series of time and Fourier series of eigenfunction. The expressions for the surface temperature and heat flux are explicitly obtained in a form of power series of time and Fourier series. The verifications for two representative testing cases have shown that the predicted surface temperature distribution is in good agreement with the prescribed surface condition, as well as the surface heat flux.

Keywords: Inverse solution; Two-dimensional heat conduction; Laplace transform; Transient

1. Introduction

A procedure to solve Inverse Heat Conduction Problems (IHCP) is to derive surface heat flux and temperature from temperature changes inside a solid. The method proves to be very powerful and useful when a direct measurement of surface heat flux and temperature is difficult, due to severe working conditions, such as those in space vehicle atmosphere re-entry, in accidents involving coolant breaks in the plasma-facing components, and in the quenching of a high temperature surface. Recently, the IHCP has been numerically treated and extended to multiple dimensions with the help of the development of computer technologies related to software and hardware and the improvement of computer capability. For example, Hsieh and Su [1] and Bell [2] employed a differential method; Lithouhi and Beck [3] employed a finite element method and Shoji and Ono [4] employed a boundary element method, to formalize two-dimensional IHCP. Moreover, Huang and Tsai [5] carried out an analysis to arbitrary boundary condition estimation inverse problems by using the conjugate gradient method. The numerical computation, although it may be efficient in achieving the inverse result, can not supply us with enough information to understand the characteristics of the solution and the effect of the influencing factors. The characteristics of inverse solution for IHCPs and different approaches are reported [6,7].

Compared to the numerical computation method, analytical methods to IHCPs could be applied only to samples with simple geometrical configurations [8–10], for which the solution may be simple and explicit. However, they still attract us greatly due mainly to two important aspects: (1) the characteristics of the whole solution can be grasped easily; and (2) the time needed for calculation is rather short. Using the Laplace transform technique, Imber [9] proposed an approximate solution in two-dimensional cylindrical geometry, which, unfortunately, is of low accuracy and therefore not for practical applications. More recently, with the same technique and a half polynomial power series of

* Corresponding author. Tel.: +81-952-28-8608; fax: +81-952-28-8587.
E-mail address: monde@me.saga-u.ac.jp (M. Monde).

0017-9310/03/$ - see front matter
doi:10.1016/S0017-9310(02)00510-0

Nomenclature

A_j	coefficients in Eq. (7)
a	thermal diffusivity
B_j	coefficients in Eq. (7)
b_k	coefficients in Eq. (8)
C_j	coefficients in Eq. (6)
c_j	coefficients in Eq. (8)
C'_1, C'_2, C'_3, C'_4	coefficients in Eq. (3)
$D^{(n)}_{j,k}$	coefficients for approximating measured temperature variation in Eq. (9)
$G^{(1)}_{j,k}$	coefficients in Eq. (18) for set 1
$G^{(1,m)}_{j,k}$	coefficients in Eq. (19) for set 2
$H^{(1)}_{j,k}$	coefficients in Eq. (22) for set 1
$H^{(1,m)}_{j,k}$	coefficients in Eq. (23) for set 2
$f(\xi,\eta_n,\tau)$	function for approximating temperatures on a line $\eta=\eta_n$
L	aspect ratio ($=L_x/L_y$)
L_x	length of a solid in x direction
L_y	length of a solid in y direction
m_j	eigenvalue ($m_j=j\pi$)
n_j	constant $\left(=i\sqrt{s+m_j^2}\right)$
N	degree of approximate polynomial with time
N_j	degree of eigenvalue
N_{sf}	order of significant figure
s	Laplace operator ($s=-(m_j^2+n_j^2)$)
T	temperature
t	dimensional time
T_c	representative temperature
x,y	spatial coordinates
Φ	dimensionless heat flux
θ	dimensionless temperature (T/T_c)
τ	dimensionless time ($=at/L_x^2$)
τ_i^*	dimensionless time lag
ξ	dimensionless distance in x direction (x/L_x)
η	dimensionless distance in y direction (y/L_y)

time in measured temperature approximation, Monde and Mitsutake [10] proposed an approximate solution for one-dimensional IHCP, which predicts the surface temperature and heat flux with high accuracy. Compared to the conventional analytical method, the Monde [10] solution is advanced in both stability and reduction in minimum predictable time.

The above Monde solution [10] has also been successfully applied to the measurement of thermal diffusivity [11]. Compared to the conventional method, in which measurement accuracy is strongly affected by a set boundary condition, the measurement using the inverse solution possesses an advantage that it is independent from the set boundary condition and thereby, is very easy to handle.

On the base of the same method as that used in Monde one-dimensional IHCP solution [10], this paper extends the method to two-dimensional systems. Analytical inverse solutions are sought for two simple cases. The method is verified by two simple cases on its applicability and main characteristics.

2. Formulation of two-dimensional inverse heat conduction problems

For a homogeneous rectangular sample, the mathematical formulation of the two-dimensional heat conduction problem can be written in a dimensionless form as

$$\frac{\partial\theta}{\partial\tau}=\frac{\partial^2\theta}{\partial\xi^2}+L^2\frac{\partial^2\theta}{\partial\eta^2}\quad 0<\xi<1,\ 0<\eta<1 \tag{1}$$

2.1. General solution for the two-dimensional unsteady heat conduction for two simplest sets of boundary conditions

Assuming a uniform initial temperature ($\theta=0$) and applying the Laplace transform to Eq. (1), we obtain in subsidiary form as

$$\frac{\partial^2\bar{\theta}}{\partial\xi^2}+L^2\frac{\partial^2\bar{\theta}}{\partial\eta^2}-s\bar{\theta}=0 \tag{2}$$

A general elementary solution is [12]

$$\bar{\theta}(\xi,\eta,s)=\left\{C'_1\cos(m\xi)+C'_2\sin(m\xi)\right\}\times\left\{C'_3\cos(n\eta/L)+C'_4\sin(n\eta/L)\right\} \tag{3}$$

where m and n are eigenvalues to be determined and satisfy the relation $m^2+n^2=-s$. C'_1, C'_2, C'_3 and C'_4 are integral constants which depend upon the boundary conditions; therefore, four individual boundary conditions are needed, on the four surfaces. To simplify the question, we only consider two simplest boundary sets.

Boundary set 1. As shown in Fig. 1, three surfaces are adiabatic and only one surface boundary condition is left unknown, which corresponds then to the IHCP solution under analysis:

$$\frac{\partial\bar{\theta}}{\partial\xi}=0\quad\text{at }\xi=0\text{ and }\xi=1 \tag{4a}$$

$$\frac{\partial\bar{\theta}}{\partial\eta}=0\quad\text{at }\eta=1 \tag{4b}$$

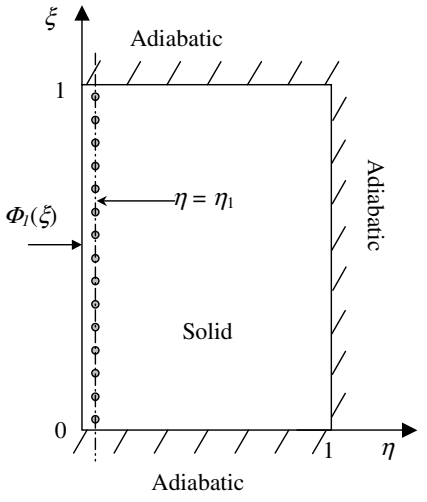

Fig. 1. Illustration of the B.C in the boundary set 1.

Boundary set 2. As shown in Fig. 2, surfaces at $\xi = 0$ and $\xi = 1$ are adiabatic and two boundary conditions on surfaces $\eta = 0$ and $\eta = 1$ are unknown:

$$\frac{\partial\bar{\theta}}{\partial\xi} = 0 \quad \text{at } \xi = 0 \text{ and } \xi = 1 \tag{5}$$

General solutions for the two boundary sets are given in subsidiary form by Eqs. (6) and (7), respectively.

$$\bar{\theta}(\xi,\eta,s) = \sum_{j=0}^{\infty} C_j \cos(m_j\xi)\cos\left\{\frac{n_j}{L}(1-\eta)\right\} \tag{6}$$

$$\bar{\theta}(\xi,\eta,s) = \sum_{j=0}^{\infty} \cos(m_j\xi)\{A_j \sin(n_j(\eta-\eta_1)/L) + B_j\cos(n_j(\eta-\eta_2)/L)\} \tag{7}$$

where m_j $(= j\pi)$ are the eigenvalues to satisfy Eq. (4a) or (5), $\cos(m_j\xi)$ are the corresponding eigenfunctions. Each value of n_j is determined from the relation of $m_j^2 + n_j^2 = -s$. The unknown constants C_j in Eq. (6) are determined using the temperature distribution measured on one line $(\eta = \eta_1)$ inside the solid (Fig. 1), whereas the constants A_j and B_j in Eq. (7) are determined by the measured temperatures on two different lines $(\eta = \eta_1$ and $\eta = \eta_2)$ inside the solid (see Fig. 2).

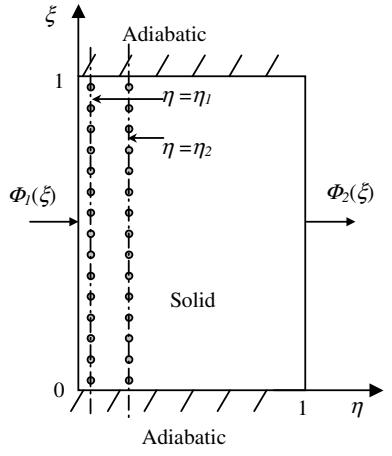

Fig. 2. Illustration of the B.C in the boundary set 2.

In general, the boundary set 2 is more commonly encountered in practice than the boundary set 1. The reason the boundary set 1 is discussed is that the number of the measuring points can be reduced by half, which is important in practical measurements. Although in the boundary set 2, there are two unknown boundary surfaces, we are interested on study only one of them; therefore, the inverse solution will only be derived for the surface of $\eta = 0$.

One of the most important characteristics of the IHCP is that the first measuring line $(\eta = \eta_1)$ should be positioned as near as possible to the unknown boundary surface, to ensure that any disturbance occurring on the unknown boundary surface can be sensed in time. If the first measuring line $(\eta = \eta_1)$ is too far away from the unknown boundary surface, it becomes impossible to sense any delicate surface disturbance and consequently results in a wrong IHCP estimation. How the positions of the measuring lines influence inverse solution will be discussed later in detail.

2.2. Approximate equation depicting temperature responses on lines η_1 and η_2

In order to determine the constants C_j, A_j and B_j in Eqs. (6) and (7), we need to formulate the measured temperature at the lines $\eta = \eta_1$ and $\eta = \eta_2$. As shown in Eq. (8), the temperature variations with coordinate of ξ and time of τ are expressed in forms of eigenfunction $\cos(m_j\xi)$ and half polynomial series, respectively.

$$f(\xi,\eta_n,\tau) = \sum_{j=0}^{N_j} c_j\cos(m_j\xi)\sum_{k=0}^{N}\frac{b_k^{(n)}}{\Gamma(k/2+1)}(\tau-\tau_n^*)^{k/2} \tag{8}$$

where c_j and $b_k^{(n)}$ are coefficients, and Γ is the gamma function [10]. The time, τ_n^*, is a time lag, determined from $\mathrm{erfc}(\eta_n/(2\sqrt{\tau_n^*})) = \min(\theta)$, which is the readable minimum division of temperature in temperature-measuring instrument.

There are two main reasons to adopt the form of half polynomial series of time: (1) the general solution of the heat conduction problem is dependent on the square of time; (2) one-dimensional IHCP using the form of half polynomial series of time has obtained the temperature approximation with good accuracy.

Naturally, one may expect the coefficients in Eq. (8), i.e., c_j and $b_k^{(n)}$, could be determined separately by using,

for example, the mean least squares method. However, since ξ and τ are not orthogonal system, the values of c_j and $b_k^{(n)}$ on two-dimensional regression plane of ξ and τ cannot be separately determined. To alleviate this difficulty, we introduce coefficients $D_{j,k}^{(n)}$, which is defined as $D_{j,k}^{(n)} = c_j b_k^{(n)}$, to substitute the coefficients c_j and $b_k^{(n)}$. Eq. (8) then is rewritten as

$$f(\xi,\eta_n,\tau) = \sum_{j=0}^{N_j}\sum_{k=1}^{N}\cos(m_j\xi)\frac{D_{j,k}^{(n)}}{\Gamma(k/2+1)}(\tau-\tau_n^*)^{k/2} \tag{9}$$

where subscripts j and k in $D_{j,k}^{(n)}$ represent the coefficients related to eigenvalues and the order of the half polynomial series of time. The superscript (n) represents the coefficients are derived from the measured temperature on line η_1 or η_2.

The increase in both numbers of eigenvalue, N_j, and the half polynomial series, N, mathematically makes Eq. (9) approach to the measured temperature better on ξ and τ coordinates [13]. However, the measured temperatures always include some error that hinders Eq. (9) to uniformly approach the measured ones with increasing the numbers of j and k. In one-dimensional case, the number of N was recommended to be smaller than 8, namely $N \leqslant 8$, in which good accuracy of the estimation was guaranteed [10]. Therefore, the number of N smaller than 8 is employed in this analysis. On the other hand, the number of eigenvalue N_j is also limited by the uncertainty in measurement and the number of the measuring points, which will be discussed later.

Procedure to determine the values of $D_{j,k}^{(n)}$ from the measured temperature usually employs least mean square method, which is explained in Appendix A. Applying this procedure to the temperatures measured at the lines η_1 and η_2, respectively, we can determine each set of the coefficients $D_{j,k}^{(1)}$ and $D_{j,k}^{(2)}$. Then performing the Laplace transform in Eq. (9), we get

$$\bar{f}(\xi,\eta_n,s) = \mathrm{e}^{-s\tau_n^*}\sum_{j=0}^{N_j}\cos(m_j\xi)\sum_{k=0}^{N}D_{j,k}^{(n)}/s^{(k/2+1)}, \quad n=1,2 \tag{10}$$

2.3. Surface temperature calculation

Applying Eq. (6) to line η_1 and Eq. (7) to the lines η_1 and η_2, setting them equal to Eq. (10), and using the orthogonal property of cos function, we can determine coefficients C_j in Eq. (6), A_j and B_j in Eq. (7).

For the boundary set 1,

$$C_j = \frac{\mathrm{e}^{-s\tau_1^*}\sum_{k=0}^{N}D_{j,k}^{(1)}/s^{(k/2+1)}}{\cos\frac{n_j(1-\eta_1)}{L}} \tag{11}$$

For the boundary set 2,

$$A_j = \frac{\mathrm{e}^{-s\tau_2^*}\sum_{k=0}^{N}D_{j,k}^{(2)}/s^{(k/2+1)}}{\cos\frac{n_j(\eta_2-\eta_1)}{L}} \tag{12}$$

$$B_j = \frac{\mathrm{e}^{-s\tau_1^*}\sum_{k=0}^{N}D_{j,k}^{(1)}/s^{(k/2+1)}}{\cos\frac{n_j(\eta_1-\eta_2)}{L}} \tag{13}$$

After these manipulations, we can finally express the solutions for the temperature change inside the solid (including boundary surfaces) as

For the boundary set 1,

$$\bar{\theta}(\xi,\eta,s) = \mathrm{e}^{-s\tau_1^*}\sum_{j=0}^{N_j}\frac{\cos(m_j\xi)\cos\left\{\frac{n_j}{L}(1-\eta)\right\}}{\cos\left\{\frac{n_j}{L}(1-\eta_1)\right\}} \times\sum_{k=0}^{N}D_{j,k}^{(1)}/s^{(k/2+1)} \tag{14}$$

For the boundary set 2,

$$\begin{aligned}\bar{\theta}(\xi,\eta,s) &= \mathrm{e}^{-s\tau_1^*}\sum_{j=0}^{N_j}\frac{\sum_{k=0}^{N}\frac{D_{j,k}^{(1)}}{s^{(k/2+1)}}\sin[(n_j/L)(\eta_2-\eta)]}{\sin\{(n_j/L)(\eta_2-\eta_1)\}}\cos(m_j\xi)\\ &\quad-\mathrm{e}^{-s\tau_2^*}\sum_{j=0}^{N_j}\frac{\sum_{k=0}^{N}\frac{D_{j,k}^{(2)}}{s^{(k/2+1)}}\sin\{(n_j/L)(\eta_1-\eta)\}}{\sin\{(n_j/L)(\eta_2-\eta_1)\}}\cos(m_j\xi)\end{aligned} \tag{15}$$

Substitution of $n_j = i\sqrt{(s+m_j^2)}$ into $\cos(n_j/L)$ and $\sin\{n_j/L(\eta_2-\eta)\}$ turns them into $\cosh\left[\sqrt{(s+m_j^2)}/L\right]$ and $i\sinh\left[\sqrt{(s+m_j^2)}/L\right]$, respectively. Taking into account these relations and setting $\eta = 0$ in Eqs. (14) and (15), we can obtain the surface temperature ($\eta = 0$) as

For the boundary set 1,

$$\bar{\theta}_w(\xi,s) = \mathrm{e}^{-s\tau_1^*}\sum_{j=0}^{N_j}\frac{\cos(m_j\xi)\cosh\left(\frac{\sqrt{s+m_j^2}}{L}\right)}{\cosh\left\{\frac{\sqrt{s+m_j^2}}{L}(1-\eta_l)\right\}} \times\sum_{k=0}^{N}D_{j,k}^{(1)}/s^{(k/2+1)} \tag{16}$$

For the boundary set 2,

$$\begin{aligned}\bar{\theta}_w(\xi,s) &= \mathrm{e}^{-s\tau_1^*}\sum_{j=0}^{N_j}\frac{\sinh\left\{\left(\sqrt{s+m_j^2}/L\right)\eta_2\right\}\cos(m_j\xi)}{\sinh\left\{\left(\sqrt{s+m_j^2}/L\right)(\eta_2-\eta_1)\right\}}\sum_{k=0}^{N}\frac{D_{j,k}^{(1)}}{s^{(k/2+1)}}\\ &\quad-\mathrm{e}^{-s\tau_2^*}\sum_{j=0}^{N_j}\frac{\sinh\left\{\left(\sqrt{s+m_j^2}/L\right)\eta_1\right\}\cos(m_j\xi)}{\sinh\left\{\left(\sqrt{s+m_j^2}/L\right)(\eta_2-\eta_1)\right\}}\sum_{k=0}^{N}\frac{D_{j,k}^{(2)}}{s^{(k/2+1)}}\end{aligned} \tag{17}$$

Expanding the hyperbolic functions in Eqs. (16) and (17) in series around $s = 0$, and then performing the inverse Laplace transform of the resulting expressions, we can get the unknown surface temperatures

For the boundary set 1,

$$\theta_w(\xi,\tau) = \sum_{j=0}^{N_j}\sum_{k=-1}^{N} \frac{G_{j,k}^{(1)}\cos(m_j\xi)}{\Gamma(k/2+1)}(\tau-\tau_1^*)^{k/2} \tag{18}$$

For the boundary set 2,

$$\theta_w(\xi,\tau) = \sum_{j=0}^{N_j}\sum_{k=-1}^{N} \frac{G_{j,k}^{(1,2)}\cos(m_j\xi)}{\Gamma(k/2+1)}(\tau-\tau_1^*)^{k/2} - \sum_{j=0}^{N_j}\sum_{k=-1}^{N} \frac{G_{j,k}^{(2,1)}\cos(m_j\xi)}{\Gamma(k/2+1)}(\tau-\tau_2^*)^{k/2} \tag{19}$$

The detailed procedures to calculate the coefficients of $G_{j,k}^{(1)}$, $G_{j,k}^{(1,2)}$ and $G_{j,k}^{(2,1)}$ in Eqs. (18) and (19) are given in Appendix B.

2.4. Surface heat flux calculation

By differentiating Eqs. (14) and (15) with respect to η, the heat flux in η direction can be derived and then the surface heat flux is obtained by setting $\eta = 0$.

For the boundary set 1,

$$\overline{\Phi}_w(\xi,s) = \mathrm{e}^{-s\tau_1^*}\sum_{j=0}^{N_j} \times \frac{\frac{\sqrt{s+m_j^2}}{L}\cos(m_j\xi)\sinh\left(\frac{\sqrt{s+m_j^2}}{L}\right)}{\cosh\left\{\frac{\sqrt{s+m_j^2}}{L}(1-\eta_l)\right\}} \times \sum_{k=0}^{N} D_{j,k}^{(1)}/s^{(k/2+1)} \tag{20}$$

For the boundary set 2,

$$\overline{\Phi}_w(\xi,s) = \mathrm{e}^{-s\tau_1^*}\sum_{j=0}^{N_j} \times \frac{\sqrt{s+m_j^2}/L\cosh\left\{\left(\sqrt{s+m_j^2}/L\right)\eta_2\right\}}{\sinh\left\{\left(\sqrt{s+m_j^2}/L\right)(\eta_2-\eta_1)\right\}} \times \sum_{k=0}^{N}\frac{D_{j,k}^{(1)}}{s^{(k/2+1)}}\cos(m_j\xi) - \mathrm{e}^{-s\tau_2^*} \times \sum_{j=0}^{N_j}\frac{\sqrt{s+m_j^2}/L\cosh\left\{\left(\sqrt{s+m_j^2}/L\right)\eta_1\right\}}{\sinh\left\{\left(\sqrt{s+m_j^2}/L\right)(\eta_2-\eta_1)\right\}} \times \sum_{k=0}^{N}\frac{D_{j,k}^{(2)}}{s^{(k/2+1)}}\cos(m_j\xi) \tag{21}$$

In the same way that we derived the surface temperature, in achieving the surface heat flux, we also need to expand the hyperbolic functions in Eqs. (20) and (21) in series around $s = 0$, and then perform the inverse Laplace transform. The unknown surface heat fluxes are finally expressed as

For the boundary set 1,

$$\Phi_w(\xi,\tau) = \sum_{j=0}^{N_j}\sum_{k=-1}^{N} \frac{H_{j,k}^{(1)}\cos(m_j\xi)}{\Gamma(k/2+1)}(\tau-\tau_1^*)^{k/2} \tag{22}$$

For the boundary set 2,

$$\Phi_w(\xi,\tau) = \sum_{j=0}^{N_j}\sum_{k=-1}^{N} \frac{H_{j,k}^{(1,2)}\cos(m_j\xi)}{\Gamma(k/2+1)}(\tau-\tau_1^*)^{k/2} - \sum_{j=0}^{N_j}\sum_{k=-1}^{N} \frac{H_{j,k}^{(2,1)}\cos(m_j\xi)}{\Gamma(k/2+1)}(\tau-\tau_2^*)^{k/2} \tag{23}$$

The detailed manipulations to calculate coefficients $H_{j,k}^{(1)}$, $H_{j,k}^{(1,2)}$ and $H_{j,k}^{(2,1)}$ in Eqs. (20) and (21) is presented in Appendix B.

For the boundary set 2, the temperature and heat flux distribution at $\eta = 1$ is out of our interest. Actually, any unknown boundary surface can be predicted from the above developed solutions by defining the unknown surface as $\eta = 0$ in advance.

3. Verification of the proposed method

In order to verify the applicability of Eqs. (18) and (22) and Eqs. (19) and (23), we need the temperatures measured on one or two lines inside the solid. In this paper, the temperature calculated from a direct solution is used as the measured temperature. As actual temperatures measured always include some uncertainty, we superimpose a random error with a normal distribution on the exact value of the temperature as given by

$$\theta(\xi,\eta_n,\tau) = \theta_{\mathrm{exact}}(\xi,\eta_n,\tau)(1+0.5\times 10^{-N_{\mathrm{sf}}}\varepsilon) \tag{24}$$

where θ_{exact} is the exact temperature calculated from a corresponding direct solution, N_{sf} is the number of significant figures and ε is a random number generated with a normal distribution ($\sigma = 1.0$) and zero mean ($m = 0$). Generally, for a temperature measurement with thermocouples, N_{sf} can be taken as 2 or 3 at most.

Because the boundary set 1 can be considered as a special case of the boundary set 2 (the heat flux on the boundary surface defined at $\eta = 1$ in Fig. 2 is 0), the solutions for the boundary set 2, Eqs. (23) and (19), can also be applied to the problems with the boundary set 1. Therefore, the following two test cases with the first boundary set can be used in both verifications of the solutions for the boundary sets 1 and 2. The boundary

conditions at $\eta = 0$ are prescribed, respectively, as Eqs. (25) and (26). The two test cases are tentatively employed, since the direct solutions for these cases are derived relatively easier, that are given in Appendix C.

Testing case 1:

$$\theta = 1 \text{ for } 0 < \xi < 0.5 \quad \text{and} \quad \theta = 0 \text{ for } 0.5 < \xi < 1.0 \quad \text{at } \eta = 0 \tag{25}$$

Testing case 2:

$$\Phi = 1 \text{ for } 0 < \xi < 0.5 \quad \text{and} \quad \Phi = 0 \text{ for } 0.5 < \xi < 1.0 \quad \text{at } \eta = 0 \tag{26}$$

Fig. 3 shows the temperature distribution at $\eta_1 = 0.02$ for the testing case 2, after being superimposed a random error. The temperatures are used to determine the coefficients $D_{j,k}^{(1)}$ in Eq. (9). Fig. 4 shows the difference in temperatures between those in Fig. 3 and reproduced by Eq. (9) using the determined coefficients $D_{j,k}^{(1)}$.

It is found from Fig. 4 that the measured temperatures are correctly approximated by Eq. (9), which may be artificially superimposed as the random error. Fig. 5 shows the estimated surface heat flux obtained with Eq. (23) for the testing case 2. The temperatures used in the calculations are on two lines at $\eta_1 = 0.02$ and $\eta_2 = 0.05$. The numbers of the terms, N_j and N used in Eq. (9) are 30 and 5, respectively. The order of significant figures N_{sf} is set at 3, which may be considered a fair level of noise in temperature measurements with thermocouples.

Fig. 6 shows the estimated surface temperature obtained with Eq. (18) for the testing case 1. Fig. 7 shows the estimated surface heat flux obtained with Eq. (22) for the testing case 2. The temperatures used in the

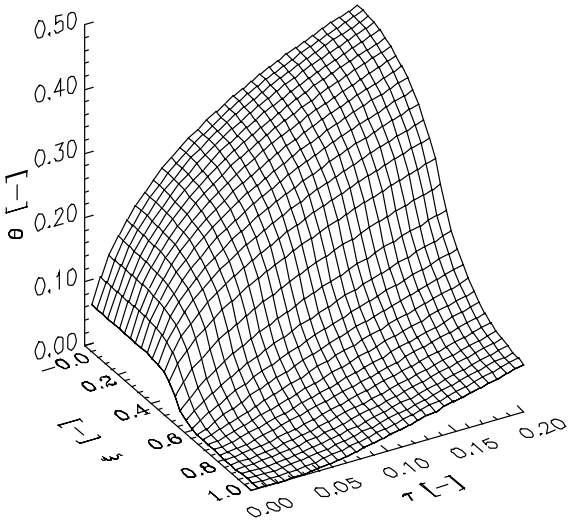

Fig. 3. Temperature distribution at $\eta_1 = 0.02$ for the testing case 2, after being superposed random error with a normal distribution.

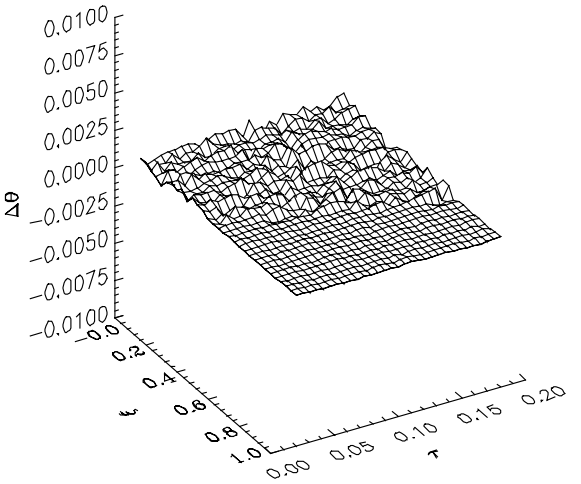

Fig. 4. Temperature reproduced from Eq. (9) for the temperature distribution in the Fig. 3.

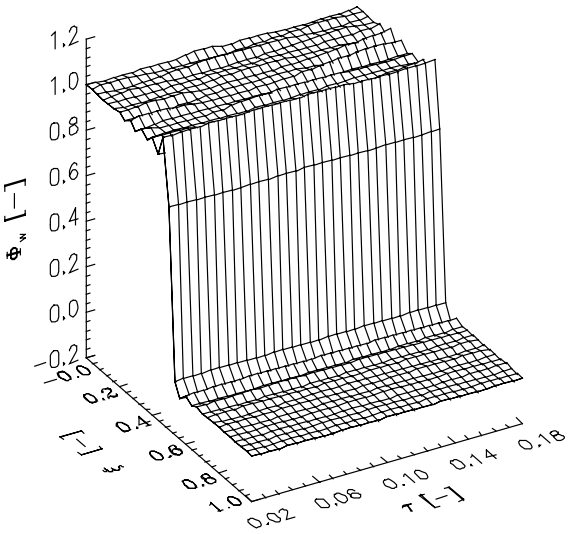

Fig. 5. Surface heat flux estimated with Eq. (23) for the testing case 2 at $\eta_1 = 0.02$ and $\eta_2 = 0.05$.

calculation are on the line $\eta_1 = 0.02$. The numbers of N_j, N and N_{sf} are kept as the same as those used in the previous calculation, that is, $N_j = 30$, $N = 5$ and $N_{sf} = 3$.

Fig. 5 shows that the surface heat flux estimated with Eq. (23) approaches the given surface heat flux and agrees with it within an error of a few percent after a time corresponding to the Fourier number $\tau = 0.02$. For the surface temperature estimated by Eq. (22), it is found from Fig. 6 that the whole surface temperatures are well predicted in an error less than 1%, although the estimated surface temperature seems to be deviating slightly from the given temperature near the discontinuity point of $\xi = 0.5$. For the testing case 2, the inverse solution,

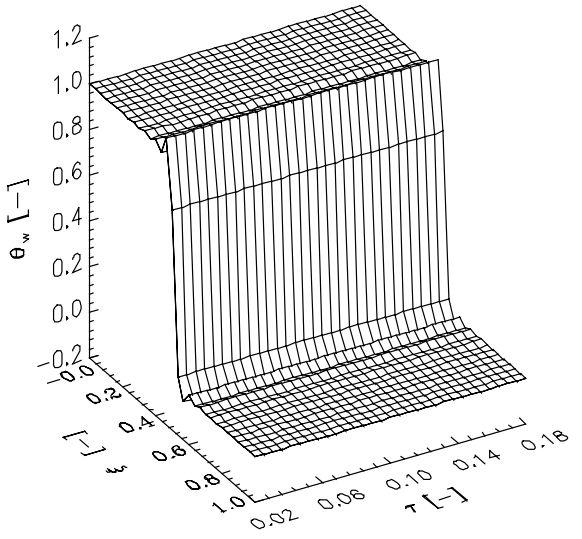

Fig. 6. Surface temperature estimated by Eq. (18) for the testing case 1 at $\eta_1 = 0.02$ and $\eta_2 = 0.05$.

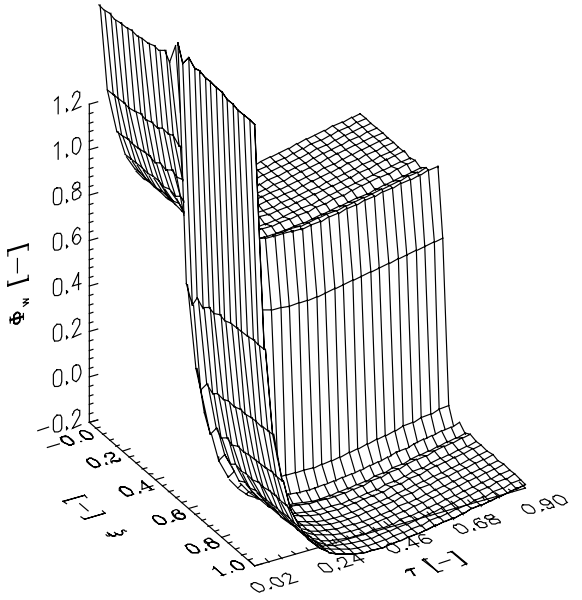

Fig. 7. Surface heat flux estimated by Eq. (22) for the testing case 2 at $\eta_1 = 0.02$ and $\eta_2 = 0.05$.

Eq. (19), predicts the surface temperature very well within an error band of 1%, because no temperature discontinuity point exists at the surface. However, the existence of the discontinuity for the surface heat flux at $\xi = 0.5$ makes estimation degrade obvious, and the estimated values present an error close 10% in the vicinity of $\xi = 0.5$, as shown in Fig. 5. The overall prediction, however, despite the existence of the discontinuity point, is still considered to be satisfactorily accuracy.

To both the testing cases 1 and 2, the inverse solutions of Eqs. (19) and (23) are capable of predicting the surface temperature and heat flux within an error bound from 3% to 5%. In general, the prediction of the surface temperature is better than that of the surface heat flux. The main reason is related to the temperature disturbance imposed by Eq. (24): For the heat flux, the temperature difference between the measuring points becomes important and it makes level of significant figure degrade, that is the imposed disturbance be amplified.

It is necessary to mention that for the testing case 1, the temperature on the surface possesses a discontinuity point at $\xi = 0.5$ so that the surface heat flux obtained by differentiating the temperature with respect to η does not converge uniformly at $\xi = 0.5$. Consequently, the predicted surface heat flux at $\xi = 0.5$ is, of course, divergent. Under such circumstances, only the temperature estimation is possible from the inverse solution, which is shown in Fig. 6. Although the surface temperature for the testing case 2 predicted from Eq. (18) is slightly inferior to that predicted from Eq. (19), it is much better than the predicted surface heat flux shown in Fig. 7.

It can be concluded from a direct comparison of Figs. 5–7 that the inverse solutions obtained from two measuring lines can estimate the surface temperature, as well as the surface heat flux, with much higher accuracy than that obtained from only one measuring line. Therefore, we recommend Eq. (23), instead of Eq. (22), to be used in the unknown surface heat flux predictions even under the boundary set 1 condition.

4. Discussions

4.1. Influence of discontinuous point

As shown in Figs. 4 and 5, a degradation of prediction accuracy is observed near the discontinuity point. The reason is attributed to the employment of the Fourier series in the temperature approximation given by Eq. (9). In other words, the Gibbs phenomenon, which is a characteristic phenomenon in the Fourier series [13], becomes apparent near the discontinuity point of $\xi = 0.5$. But, for the location far from the discontinuity, the present inverse solution is still available.

4.2. Minimum predictable time

Eqs. (16) and (22) and Eqs. (19) and (23) give out the surface temperature and heat flux explicitly. However, based on study of one-dimensional IHCP [10], we expect that for the Laplace operator, s, Eq. (11) could become divergent. This characteristic takes place in any inverse solution including numerical and analytical ones, that is mathematically verified [6,7], since it takes a time for a

sensor located at a position in solid to get a signal of the temperature change. In the inverse Laplace transform, there necessarily exists a minimum time, only after which the inverse solutions become applicable. In other words, only after the minimum time τ_{min}, the inverse solutions developed near $s = 0$ become predictable. In the present solutions, the minimum time is about $\tau_{min} = 0.02$, which can be observed from Figs. 5 and 6.

4.3. Influence of the number of eigenvalue N_j and of N

The improvement of the temperature approximation accuracy in Eq. (9) is considered to be the most important and effective way to improve the accuracy of the whole IHCP estimation. Because Eq. (9) is formulated using the Fourier series composed of eigenfunctions, $\cos(j\pi\xi)$, we may expect to improve the temperature approximation accuracy through increasing the number of eigenvalues N_j. However, higher order terms require an increase in the number of measuring points, which may cause inconvenience and difficulties in actual experimental processes. In addition, the higher order terms in the Fourier series usually makes their values diverge due to the uncertainties in the measured temperature, although in the case of error-free values they theoretically converge and become less important in the whole series. Therefore, the higher the number of eigenvalue N_j does not lead to a better solution when the measured temperatures with an error are employed. The influence of N_j on the accuracy is dependent upon the error in the measured data.

To check a possible influence of the number of eigenvalues N_j, we increased the number to 40. No obvious improvement of the accuracy was observed. In the future, the accuracy improvement due to the increase of N_j needs to be examined with concerning the accuracy of the measured temperature.

As for the number of eigenvalue N_j, Monde and Mitsutake [10] recently reported that for the case of one-dimensional IHCP, the number of N, which is the order of the half polynomial series of time used in approximating temperature changes, has to range from 5 to 8, otherwise no improvement is expected.

4.4. Influence of the relative positions of the two temperature measuring lines

To check the influence of the relative positions of the two temperature measuring lines, we further set the positions of the two measuring lines to

Combination 1: $\eta_1 = 0.05$ and $\eta_2 = 0.10$;
Combination 2: $\eta_1 = 0.02$ and $\eta_2 = 0.10$.

With keeping N_j, N and N_{sf} the same as that used in the estimation of Fig. 5, we can obtain the estimations for the combinations 1 and 2. The results are shown, respectively, in Figs. 8 and 9.

When compared to Fig. 5, which is derived under $\eta_1 = 0.02$ and $\eta_2 = 0.05$, the increase of both distances from the two measuring lines to the boundary surface (combination 1) degrades estimation to an error level around 10%, as shown in Fig. 8. Then keeping the second measuring line in the same position ($\eta_2 = 0.10$) and shifting the first measuring line closer to the boundary surface ($\eta_1 = 0.02$), the estimation is improved to an error level around 5%, as shown in Fig. 9. Furthermore,

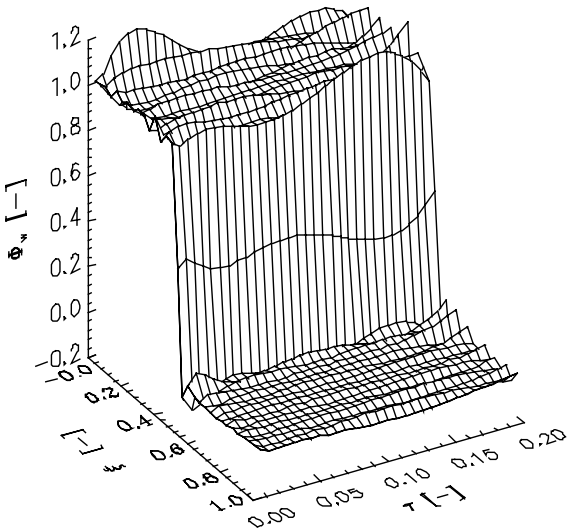

Fig. 8. Surface heat flux estimated by Eq. (23) for the testing case 2 at $\eta_1 = 0.05$ and $\eta_2 = 0.10$.

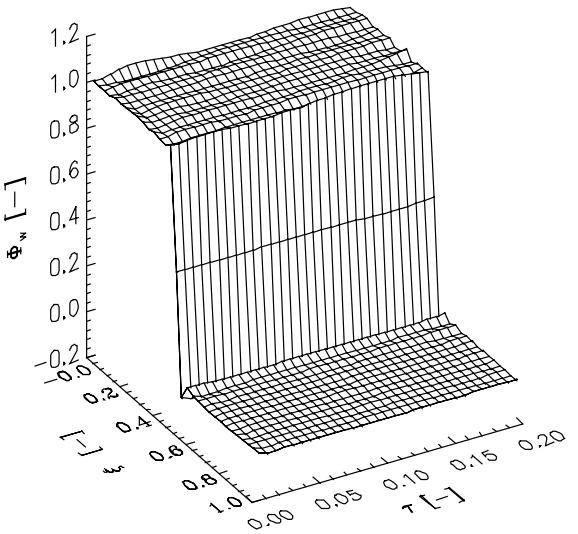

Fig. 9. Surface heat flux estimated by Eq. (23) for the testing case 2 at $\eta_1 = 0.02$ and $\eta_2 = 0.10$.

when the first measuring line is kept at the same position ($\eta_1 = 0.02$) and the second measuring line is distanced to 0.20, no obvious degradation is observed in the estimation result.

Therefore, only the position of the first measuring line is considered to be significantly relative to the estimation accuracy. The first measuring line should be positioned as near as possible to the unknown boundary surface, to ensure all the disturbances occurring on the unknown boundary surface can be sensed in time, whereas the second measuring line can be located far away from the unknown boundary surface. The position of η_1 is recommended to be smaller than 0.02, if possible.

4.5. Influence of the temperature measurement accuracy

To check the influence of the temperature-measuring accuracy upon the prediction results, we set the number of the significant figure N_{sf} in Eq. (24) to 2, 3 and ∞ (error-free). The corresponding results are shown in Figs. 10, 5 and 11, respectively.

When N_{sf} is 2, as shown in Fig. 10, the prediction result is much poorer than that when N_{sf} is set at 3. The error in the estimation is about 20%. The IHCP solution calculated from error-free temperature data, as shown in Fig. 11, still possesses an error around 4%, which is almost the same as that calculated from $N_{sf} = 3$. This influencing tendency tells us about the importance of the accuracy of the measured data. In actual measurements, although it is unavoidable that the measured temperature contains some uncertainty, an effort of employing high precision instrument may lead directly to an improvement of predicting accuracy for the IHCP solution. If the data of $N_{sf} = 3$ are used, then the number of N is 30 enough which are too large in actual measurement. Next target may be how to reduce from $N = 30$ to a suitable number of the measuring points, from which the temperature profile can be approximated.

4.6. Discussion on the solutions for the two boundary sets

Boundary set 1 is a special case of the boundary set 2 and the solutions for the boundary set 2 can also be used for the problems with the boundary set 1. But the solutions for the boundary set 1 cannot be used for the problems with the boundary set 2. The reason the boundary set 1 is discussed is that the number of the measuring points can be reduced by half, which interests us very much in practical measurements. As the measured temperature always includes error, the decrease in the measuring points may be helpful in reducing number of the uncertainties, resulting into a better estimation. Consequently, we may get the impression that the solutions derived for the boundary set 1 gives more accurate estimation than that derived for the boundary set 2. However, the verification shown in

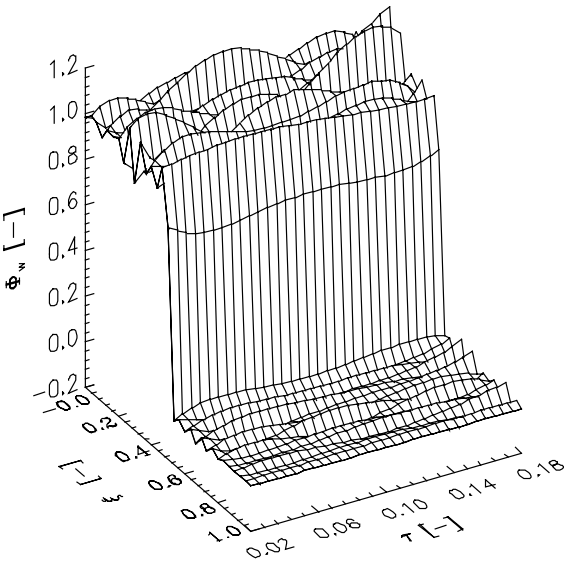

Fig. 10. Surface heat flux estimated by Eq. (23) for testing case 2 with $N_{sf} = 2$ ($\eta_1 = 0.02$ and $\eta_2 = 0.05$).

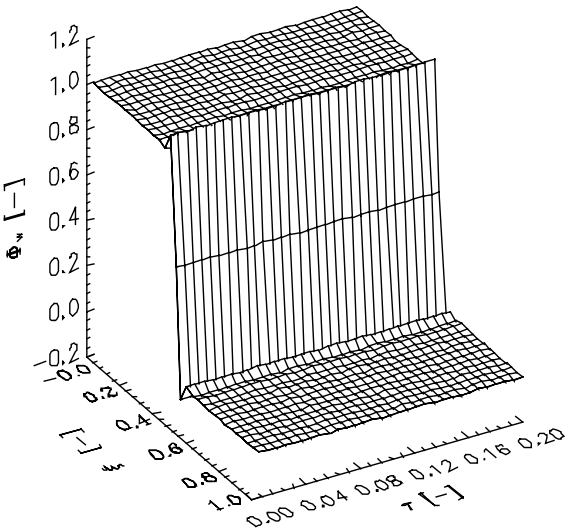

Fig. 11. Surface heat flux estimated for testing case 2 by Eq. (23) with error-free temperature data ($\eta_1 = 0.02$ and $\eta_2 = 0.05$).

Figs. 5 and 7 tells us a contrary result, that is, the inverse solution of Eq. (22) for the boundary set 1 can be available after a time of about 0.3, whereas Eq. (23) for the boundary set 2 can be available after a time of 0.02. Therefore, Eq. (23) has to be applied, instead of Eq. (22), even for problems with the boundary set 1. The reason Eq. (22) gives a worse estimation is that although the boundary condition at $\eta = 1$, being the same role as η_2, is exactly true, the position is too far (farthest) away from the interested surface.

5. Application to moving heat source

In order to check availability of the inverse solutions of Eqs. (19) and (23), one may apply them to a heat source moving along the surface, which is often encountered in engineering field such as a quench of hot surface and a conceptual emergency cooling in nuclear reactor and is one of the severest boundary condition. We consider another simple case of moving heat sources along the surface, $\eta = 0$, which is expressed as

$$\begin{aligned} \Phi_w &= 1 \quad \text{for } \xi \leqslant \tau \\ \Phi_w &= 0 \quad \text{for } \xi > \tau \end{aligned} \tag{27}$$

The direct solution for this boundary condition, which is expressed in Appendix C [14] can give temperatures on two lines of $\eta_1 = 0.02$ and $\eta_2 = 0.05$ where the measuring points on each line are set at 26. Following the same procedure, we can determine the coefficients $D_{j,k}^{(n)}$ form these temperatures with the same random error given by Eq. (24) and then calculate the needed coefficients in Eq. (23). In the present calculation, the orders of N_j and N in Eq. (23) are set at 26 and 5, respectively, and the order of significant figures is set at $N_{sf} = 3$.

Fig. 12 shows the calculated result for the moving heat source and makes it clear that the surface heat flux for the heat source moving along the surface can be predicted well within the range from $\tau = 0.02$ to 1.126 without discontinuity point around which the accuracy is degraded up to an error near 10%. It is necessary to mention that the surface temperatures are well predicted inside an error band of 1% over the whole range, since the surface temperature continuously changes. Incidentally, in order to get such a good estimation, we notice that the measured temperatures should be also approximated at a high accuracy of 0.1% by Eq. (9). However, for the case of the moving heat source that the measured temperature in the solid radically changes with time, especially at a point at which the moving heat source reaches, Eq. (9) fails in approximating the temperatures measured over the whole range of the measured time. As the result, it is found that the inverse solutions also failed high accurate prediction for both surface temperature and heat flux. Therefore, we introduce a new method in which the whole time range is divided into some subdivisions of the time and by which the measured temperature can be approximated well for each subdivision using Eq. (9). Finally, the result shown in Fig. 12 can be obtained by dividing the whole time range into eight subdivisions.

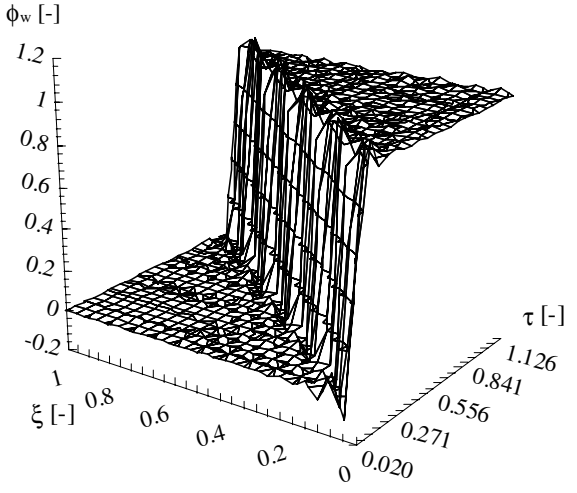

Fig. 12. Surface heat flux calculated from Eq. (23) for moving heat source using time partition method.

6. Conclusion

With using the Laplace transform technique, we achieved inverse solutions for two-dimensional IHCP for two simple boundary sets, the results are summarized as the following:

1. Except in the vicinity of discontinuity point, surface temperature and heat flux can be predicted well over the whole surface with an error less than a few percent.
2. The minimum predictive time for the proposed IHCP solution is about $\tau_{min} = 0.02$.
3. The position of the first measuring line η_1 in the solid is recommended to be as near as possible to the interested unknown boundary surface and not to be farther than 0.02.
4. Eq. (23), instead of Eq. (22), is recommended for estimating surface heat flux even for the boundary set 1 condition.
5. In order to predict the surface temperature and heat flux from the proposed IHCP solution successfully, a high precision instrument that can ensure measured temperature at uncertainty level less than 0.1%, namely $N_{sf} = 3$ at least, is recommended.

Appendix A. Procedures for determining $D_{j,k}^{(n)}$ in Eq. (9)

The determination to $D_{j,k}^{(n)}$ is the base for obtaining the inverse solution. We explain two procedures to calculate the coefficients.

Procedure 1. To a concrete measuring point ($\xi = \xi_i$) on η_n, Eq. (9) can be rewritten to

$$f(\xi_i, \eta_n, \tau) = \sum_{k=0}^{N_k} \left[\sum_{j=0}^{\infty} \cos(m_j \xi_i) \frac{D_{j,k}^{(n)}}{\Gamma(k/2+1)} \right] (\tau - \tau_n^*)^{k/2}$$

If we define $P_{j,k}^{(n)} = \sum_{j=0}^{\infty} \cos(m_j\xi_i) D_{j,k}^{(n)}$, the above equation is then rewritten to

$$f(\xi_i, \eta_n, \tau) = \sum_{k=0}^{N_k} \frac{P_{j,k}^{(n)}}{\Gamma(k/2+1)} (\tau - \tau_n^*)^{k/2}$$

When temperature change along time at a concrete measuring point ($\xi = \xi_i$) is known, coefficients $P_{j,k}^{(n)}$ ($k = 0, 1, 2, \ldots, N_k$) can be calculated from the mean least squares method. Repeat the process to all the measuring points (totally N_j points) on the line η_n, coefficients $P_{j,k}^{(n)}$ ($j = 1, 2, \ldots, N_j$ and $k = 0, 1, 2, \ldots, N_k$) are obtained and then under a constant k, calculate $D_{j,k}^{(n)}$ ($j = 1, 2, \ldots, N_j$). Repeat the process to all the possible values of k ($k = 0, 1, \ldots, N_k$), and then the coefficients $D_{j,k}^{(n)}$ ($j = 1, 2, \ldots, N_j$ and $k = 0, 1, \ldots, N_k$) can be determined. The $D_{j,k}^{(n)}$ determination procedure tells us obviously that the degree of eigenvalue is restricted by the number of the measuring points.

Procedure 2. Another way is to consider an element of $Q_{j,k}(\xi, \tau) = \cos(m_j\xi)(\tau - \tau_n^*)^{k/2}/\Gamma(k/2+1)$. The value of any element is known for the measured values of ξ and τ.

$$f(\xi, \eta, \tau) = \sum_{k=0}^{N} \sum_{j=0}^{N_j} D_{j,k}^{(n)} Q_{j,k}(\xi, \tau)$$

A set of linear equation for $D_{j,k}^{(n)}$ can be obtained for each point of (ξ_l, τ_m). These sets can be solved directly to satisfy the requirement of the mean least square by applying the modified Gram–Schmidt method, which was opened in Fortran 77 textbook.

Appendix B

The Laplace-transformed surface temperature and heat flux can be written in a form of $\bar{\theta} = \bar{f}(s)K(s)$, where $\bar{f}(s)$ and $K(s)$ are temperature approximate function and kernel function (see Table 1), respectively. To get the solution of IHCP (surface heat flux and temperature), the inverse Laplace transform, which is written in the following equation, is performed to $\bar{\theta}$:

$$\theta(\tau) = \frac{1}{2\pi \mathrm{i}} \int_{c-\mathrm{i}\infty}^{c+\mathrm{i}\infty} \mathrm{e}^{s\tau} \bar{\theta}(s)\, \mathrm{d}s$$

In this research, the above complex integral is carried out after the kernel function $K(s)$ is extended around $s = 0$. The surface temperature and heat flux then can be expressed in form of $K(s)$.

In spite of coordinate systems, kernels of $K_{1,j}(s)$ and $K_{2,j}(s)$ for the set 1 and $K_{1,j}^{(l)}(s)$ and $K_{2,j}^{(l)}(s)$ ($l = 1, 2$) for the set 2 expanded in a series around $s = 0$ are always written in a common form:

$$K_{1,j}^{(l)}(s) = \mathrm{Co}_{1,j}^{(l)} \sum_{n=0}^{\infty} c_{n,j}^{(l)} s^n$$

and

$$K_{2,j}^{(l)}(s) = \mathrm{Co}_{2,j}^{(l)} \sum_{n=0}^{\infty} d_{n,j}^{(l)} s^n, \quad l = 1, 2$$

The coefficients $c_{n,j}^{(l)}$ and $d_{n,j}^{(l)}$ are also written in similar form as

$$c_{n,j}^{(l)} = \frac{1}{g_0} \sum_{i=0}^{n} x_{i,j}^{(l)} h_{n-i,j}$$

and

$$d_{n,j}^{(l)} = \frac{1}{g_0} \sum_{i=0}^{n} y_{i,j}^{(l)} h_{n-i,j}, \quad l = 1, 2$$

where $h_{i,j}$ is calculated from the following listed equations. The calculation to the employed item $g_{i,j}$ and coefficients $x_{i,j}^{(l)}$, $y_{i,j}^{(l)}$ are listed in Table 2.

$$\begin{aligned}
h_{0,j} &= 1 \\
h_{1,j} &= -g_{1,j} \\
h_{2,j} &= -g_{2,j} + g_{1,j}^2 \\
h_{3,j} &= -g_{3,j} + 2g_{1,j}g_{2,j} - g_{1,j}^3 \\
h_{4,j} &= -g_{4,j} + (2g_{1,j}g_{3,j} + g_{2,j}^2) - 3g_{1,j}^2 g_{2,j} + g_{1,j}^4 \\
h_{5,j} &= -g_{5,j} + 2(g_{1,j}g_{4,j} + g_{2,j}g_{3,j}) - 3(g_{1,j}^2 g_{3,j} + g_{1,j}g_{2,j}^2) \\
&\quad + 4g_{1,j}^3 g_{2,j} - g_{1,j}^5 \\
&\vdots
\end{aligned}$$

With rearrangement, $\bar{\theta}_w(s)$ and $\overline{\phi}_w(s)$ are derived as:

(1) For the boundary set 1,

$$\begin{aligned}
\bar{\theta}_w(s) &= \mathrm{e}^{-s\tau_1^*} \sum_{j=0}^{N_j} \sum_{k=0}^{N} \frac{D_{j,k}^{(1)} \cos(m_j\xi)}{s^{(k/2+1)}} \sum_{n=0}^{\infty} \mathrm{Co}_{1,j} c_{n,j} s^n \\
&= \mathrm{e}^{-s\tau_1^*} \sum_{j=0}^{N_j} \sum_{k=-1}^{N} G_{j,k}^{(1)} s^n \cos(m_j\xi)
\end{aligned}$$

Table 1

	Surface temperature	Surface heat flux
Boundary set 1	$\bar{\theta} = \sum_{j=0}^{N_j} \bar{f}_1(s) K_{1,j}(s)$	$\overline{\Phi} = \sum_{j=0}^{N_j} \bar{f}_{1,j}(s) K_{2,j}(s)$
Boundary set 2	$\bar{\theta} = \sum_{j=0}^{N_j} \left\{ \bar{f}_1(s) K_{1,j}^{(2)}(s) - \bar{f}_2(s) K_{1,j}^{(1)}(s) \right\}$	$\overline{\Phi} = \sum_{j=0}^{N_j} \left\{ \bar{f}_{1,j}(s) K_{2,j}^{(2)}(s) - \bar{f}_{2,j}(s) K_{2,j}^{(1)}(s) \right\}$

$$\overline{\Phi}_w(s) = \mathrm{e}^{-s\tau_1^*}\sum_{j=0}^{N_j}\sum_{k=0}^{N}\frac{D_{j,k}^{(1)}\cos(m_j\xi)}{s^{(k/2+1)}}\sum_{n=0}^{\infty}\mathrm{Co}_{2,j}d_{n,j}s^n = \mathrm{e}^{-s\tau_1^*}\sum_{j=0}^{N_j}\sum_{k=-1}^{N}H_{j,k}^{(1)}s^n\cos(m_j\xi)$$

where

$$G_{j,-1}^{(1)} = \sum_{k=0}^{N_k}D_{j,2k+1}^{(1)}E_{j,k+1},\quad l=-1,\ N_k=\mathrm{Int}\{(N-1)/2\}$$

$$G_{j,l}^{(1)} = \sum_{k=0}^{N_k}D_{j,2k+l}^{(1)}E_{j,k},\quad 0\leqslant l\leqslant N,\ N_k=\mathrm{Int}\{(N-l)/2\}$$

$$H_{j,-1}^{(1)} = \sum_{k=0}^{N_k}D_{j,2k+1}^{(1)}F_{j,k+1},\quad l=-1,\ N_k=\mathrm{Int}\{(N-1)/2\}$$

$$H_{j,l}^{(1)} = \sum_{k=0}^{N_k}D_{j,2k+1}^{(1)}F_{j,k},\quad 0\leqslant l\leqslant N,\ N_k=\mathrm{Int}\{(N-l)/2\}$$

and $G_{j,l}^{(1)}$ and $H_{j,l}^{(1)}$ are coefficients of Eqs. (18) and (22), respectively, and $E_{j,k}=\mathrm{Co}_{1,j}c_{k,j}$ and $F_{j,k}=\mathrm{Co}_{2,j}d_{k,j}$

(2) For the boundary set 2,

$$\bar{\theta}_w(s) = \mathrm{e}^{-s\tau_1^*}\sum_{j=0}^{N_j}\sum_{k=0}^{N}\frac{D_{j,k}^{(1)}\cos(m_j\xi)}{s^{(k/2+1)}}\sum_{n=0}^{\infty}\mathrm{Co}_{1,j}^{(2)}c_{n,j}^{(2)}s^n - \mathrm{e}^{-s\tau_2^*}\sum_{j=0}^{N_j}\sum_{k=0}^{N}\frac{D_{j,k}^{(2)}\cos(m_j\xi)}{s^{(k/2+1)}}\sum_{n=0}^{\infty}\mathrm{Co}_{1,j}^{(1)}c_{n,j}^{(1)}s^n = \mathrm{e}^{-s\tau_1^*}\sum_{j=0}^{N_j}\sum_{k=-1}^{N}\frac{G_{j,k}^{(1,2)}}{s^{(k/2+1)}}\cos(m_j\xi) - \mathrm{e}^{-s\tau_2^*}\sum_{j=0}^{N_j}\sum_{k=-1}^{N}\frac{G_{j,k}^{(2,1)}}{s^{(k/2+1)}}\cos(m_j\xi)$$

Table 2
Kernel $K(s)$ and its coefficients

		Surface temperature ($K_{1,j}(s)$)	Surface heat flux ($K_{2,j}(s)$)
(1) For the boundary set 1 Kernel $K(s)$		$\dfrac{\cosh\left\{\sqrt{\left(s+m_j^2\right)}\frac{1}{L}\right\}}{\cosh\left\{\sqrt{\left(s+m_j^2\right)}\left(\frac{1-\eta_1}{L}\right)\right\}}$	$\dfrac{\frac{\sqrt{\left(s+m_j^2\right)}}{L}\sinh\left\{\sqrt{\left(s+m_j^2\right)}\frac{1}{L}\right\}}{\cosh\left\{\sqrt{\left(s+m_j^2\right)}\left(\frac{1-\eta_1}{L}\right)\right\}}$
$m_j=0$ $(j=0)$	Coefficients of $K(s)$ after expansion	$x_{n,0}=\frac{1}{(2n)!}\left(\frac{1}{L}\right)^{2n}$	$y_{0,0}=0$, $y_{n,0}=\frac{1}{(2n-1)!}\left(\frac{1}{L}\right)^{2n-1}$ $(n\geqslant 1)$
	Coefficients Co_j	$\mathrm{Co}_{1,0}=1$	$\mathrm{Co}_{2,0}=\frac{1}{L}$
	Common item	$g_{n,0}=\frac{1}{(2n)!}\left(\frac{1-\eta_1}{L}\right)^{2n}$	
$m_j>0$ $(j>0)$	Coefficients of $K(s)$ after expansion	$x_{n,j}=\dfrac{\sum_{k=n}\frac{{}_kC_n}{(2k)!}\left(\frac{1}{L}\right)^{2k}m_j^{2(k-n)}}{\cosh\left(m_j\frac{1}{L}\right)}$	$y_{0,j}=1$, $y_{n,j}=\dfrac{\sum_{k=n-1}\frac{{}_{k+1}C_n}{(2k+1)!}\left(\frac{1}{L}\right)^{2k+1}m_j^{2(k+1-n)}}{m_j\sinh\left(m_j\frac{1}{L}\right)}$ $(n\geqslant 1)$
	Coefficients Co_j	$\mathrm{Co}_{1,j}=\dfrac{\cosh\left(m_j\frac{1}{L}\right)}{\cosh\left\{m_j\left(\frac{1-\eta_1}{L}\right)\right\}}$	$\mathrm{Co}_{2,j}=\frac{1}{L}\dfrac{m_j\sinh\left(m_j\frac{1}{L}\right)}{\cosh\left\{m_j\left(\frac{1-\eta_1}{L}\right)\right\}}$
	Common item	$g_{n,j}=\dfrac{\sum_{k=n}\frac{{}_kC_n}{(2k)!}\left(\frac{1-\eta_1}{L}\right)^{2k}m_j^{2(k-n)}}{\cosh\left\{m_j\left(\frac{1-\eta_1}{L}\right)\right\}}$	
		Surface temperature ($K_{1,j}^{(l)}(s)$)	Surface heat flux ($K_{2,j}^{(l)}(s)$)
(2) For the boundary set 2 Kernel $K(s)$		$\dfrac{\sinh\left\{\sqrt{\left(s+m_j^2\right)}\frac{\eta_l}{L}\right\}}{\sinh\left\{\sqrt{\left(s+m_j^2\right)}\left(\frac{\eta_2-\eta_1}{L}\right)\right\}}$	$\dfrac{\frac{\sqrt{\left(s+m_j^2\right)}}{L}\cosh\left\{\sqrt{\left(s+m_j^2\right)}\frac{\eta_l}{L}\right\}}{\sinh\left\{\sqrt{\left(s+m_j^2\right)}\left(\frac{\eta_2-\eta_1}{L}\right)\right\}}$
$m_j=0$ $(j=0)$	Coefficients of $K(s)$ after expansion	$x_{n,0}^{(l)}=\frac{1}{(2n+1)!}\left(\frac{\eta_l}{L}\right)^{2n+1}$	$y_{n,0}^{(l)}=\frac{1}{(2n)!}\left(\frac{\eta_l}{L}\right)^{2n}$
	Coefficients Co_j	$\mathrm{Co}_{1,0}^{(l)}=1$	$\mathrm{Co}_{2,0}^{(l)}=\frac{1}{L}$
	Common item	$g_{n,0}=\frac{1}{(2n+1)!}\left(\frac{\eta_2-\eta_1}{L}\right)^{2n+1}$	
$m_j>0$ $(j>0)$	Coefficients of $K(s)$ after expansion	$x_{n,j}^{(l)}=\dfrac{\sum_{k=n}\frac{{}_kC_n}{(2k+1)!}\left(\frac{\eta_l}{L}\right)^{2k+1}m_j^{2(k-n)+1}}{\sinh\left(m_j\frac{\eta_l}{L}\right)}$	$y_{n,j}^{(l)}=\dfrac{\sum_{k=n}\frac{{}_kC_n}{(2k)!}\left(\frac{\eta_l}{L}\right)^{2k}m_j^{2(k-n)}}{\cosh(m_j\frac{\eta_l}{L})}$
	Coefficients Co_j	$\mathrm{Co}_{1,j}^{(l)}=\dfrac{\sinh\left(m_j\frac{\eta_l}{L}\right)}{\sinh\left\{m_j\left(\frac{\eta_2-\eta_1}{L}\right)\right\}}$	$\mathrm{Co}_{2,j}^{(l)}=\frac{1}{L}\dfrac{m_j\cosh\left(m_j\frac{\eta_l}{L}\right)}{\sinh\left\{m_j\left(\frac{\eta_2-\eta_1}{L}\right)\right\}}$
	Common item	$g_{n,j}=\dfrac{\sum_{k=n}\frac{{}_kC_n}{(2k+1)!}\left(\frac{\eta_2-\eta_1}{L}\right)^{2k+1}m_j^{2(k-n)+1}}{\sinh\left\{m_j\left(\frac{\eta_2-\eta_1}{L}\right)\right\}}$	

$$\overline{\Phi}_w(s) = \mathrm{e}^{-s\tau_1^*}\sum_{j=0}^{N_j}\sum_{k=0}^{N}\frac{D_{j,k}^{(1)}\cos(m_j\xi)}{s^{(k/2+1)}}\sum_{n=0}^{\infty}\mathrm{Co}_{2,j}^{(2)}d_{n,j}^{(2)}s^n - \mathrm{e}^{-s\tau_2^*}\sum_{j=0}^{N_j}\sum_{k=0}^{N}\frac{D_{j,k}^{(2)}\cos(m_j\xi)}{s^{(k/2+1)}}\sum_{n=0}^{\infty}\mathrm{Co}_{2,j}^{(1)}d_{n,j}^{(1)}s^n = \mathrm{e}^{-s\tau_1^*}\sum_{j=0}^{N_j}\sum_{k=-1}^{N}\frac{H_{j,k}^{(1,2)}}{s^{(k/2+1)}}\cos(m_j\xi) - \mathrm{e}^{-s\tau_2^*}\sum_{j=0}^{N_j}\sum_{k=-1}^{N}\frac{H_{j,k}^{(2,1)}}{s^{(k/2+1)}}\cos(m_j\xi)$$

where

$$G_{j,-1}^{(l,m)} = \sum_{k=0}^{N_k}D_{j,2k+1}^{(l)}E_{j,k+1}^{(m)},\quad l=-1,\ N_k=\mathrm{Int}\{(N-1)/2\}$$

$$G_{j,l}^{(l,m)} = \sum_{k=0}^{N_k}D_{j,2k+l}^{(l)}E_{j,k}^{(m)},\quad 0\leqslant l\leqslant N,\ N_k=\mathrm{Int}\{(N-l)/2\}$$

$$H_{j,-1}^{(l,m)} = \sum_{k=0}^{N_k}D_{j,2k+1}^{(l)}F_{j,k+1}^{(m)},\quad l=-1,\ N_k=\mathrm{Int}\{(N-1)/2\}$$

$$H_{j,l}^{(l,m)} = \sum_{k=0}^{N_k}D_{j,2k+l}^{(l)}F_{j,k}^{(m)},\quad 0\leqslant l\leqslant N,\ N_k=\mathrm{Int}\{(N-l)/2\}$$

and $G_{j,l}^{(l,m)}$ and $H_{j,l}^{(l,m)}$ are coefficients of Eqs. (19) and (23), respectively, and $E_{j,k}^{(m)}=\mathrm{Co}_{1,j}^{(m)}c_{k,j}^{(m)}$ and $F_{j,k}^{(m)}=\mathrm{Co}_{2,j}^{(m)}d_{k,j}^{(m)}$.

Appendix C. Direct solutions for three different boundary conditions

The direct solutions can be expressed as

(1) For the testing case 1,

$$\theta_{\mathrm{exact}}(\xi,\eta,t) = \frac{2}{\pi}\sum_{j=1}^{\infty}\frac{\sin(j\pi/2)\cos(j\pi\xi)}{j}\frac{\cosh\{(1-\eta)j\pi/L\}}{\cosh(j\pi/L)} - \frac{2}{\pi^3}\sum_{j=1}^{\infty}\sum_{k=0}^{\infty}2\frac{\sin(j\pi/2)\cos(j\pi\xi)}{j} \times\frac{L^2\pi(2k+1)\sin\{(2k+1)\eta\pi/2\}\,\mathrm{e}^{-\left(\frac{L^2}{4}(2k+1)^2+j^2\right)\pi^2 t}}{\{L^2(2k+1)^2/4+j^2\}} + \frac{1}{2}-\frac{2}{\pi}\sum_{k=0}^{\infty}\frac{\sin\{(2k+1)\eta\pi/2\}\,\mathrm{e}^{-(L^2(2k+1)^2/4)\pi^2 t}}{(2k+1)}$$

(2) For the testing case 2,

$$\theta_{\mathrm{exact}} = \frac{1}{2}\left(\frac{1}{2!}(1-\eta)^2+t-\frac{1}{3!}\right) - \frac{1}{\pi^2}\sum_{k=1}^{\infty}\frac{L^2\cos(k\pi\eta)\,\mathrm{e}^{-(Lk\pi)^2 t}}{k^2} + \frac{2L}{\pi^2}\sum_{n=0}^{\infty}(-1)^n\frac{\cos\{(2n+1)\pi\xi\}}{(2n+1)} \times\frac{\cosh\{(2n+1)\pi(1-\eta)/L\}}{\sinh\{(2n+1)\pi/L\}} - \frac{2L^2}{\pi^2}\sum_{n=0}^{\infty}(-1)^n\frac{\cos\{(2n+1)\pi\xi\}\,\mathrm{e}^{-(2n+1)^2\pi^2 t}}{(2n+1)^2} - \frac{4L^2}{\pi^3}\sum_{n=0}^{\infty}\sum_{k=1}^{\infty}(-1)^n \times\frac{\cos\{(2n+1)\pi\xi\}\cos(k\eta\pi)\mathrm{e}^{-[(2n+1)^2+(Lk)^2]\pi^2 t}}{\{(2n+1)^2+(Lk)^2\}(2n+1)}$$

(3) For the moving heat source [14],

$$\theta(\xi,\eta,\tau) = \theta_1(\xi,\eta,\tau)+\theta_2(\xi,\eta,\tau)+\theta_3(\xi,\eta,\tau)+\theta_4(\xi,\eta,\tau)$$

where

$$\theta_1(\xi,\eta,\tau) = C_1q_0b\frac{\tau^2}{2}$$

$$\theta_2(\xi,\eta,\tau) = \sum_{j=1}^{\infty}2C_1q_0L^2\frac{\cos(j\pi\xi)}{(j\pi)^4+(j\pi b)^2}\left(j\pi\sin(j\pi b\tau)-b\times\cos(j\pi b\tau)+b\mathrm{e}^{-(j\pi)^2\tau}\right)$$

$$\theta_3(\xi,\eta,\tau) = \sum_{k=1}^{\infty}2C_1q_0b\frac{\cos(k\pi\eta)}{(k\pi)^2}\left(\tau-\frac{1}{(Lk\pi)^2}+\frac{1}{(Lk\pi)^2}\mathrm{e}^{-(Lk\pi)^2\tau}\right)$$

$$\theta_4(\xi,\eta,\tau) = \sum_{j=1}^{\infty}\sum_{k=1}^{\infty}4C_1q_0L^2\frac{\cos(j\pi\xi)\cos(k\pi\eta)}{((j\pi)^2+(Lk\pi)^2)^2+(j\pi b)^2}\times\left(\frac{(j\pi)^2+(Lk\pi)^2}{j\pi}\sin(j\pi b\tau)-b\cos(j\pi b\tau)+b\mathrm{e}^{-[(j\pi)^2+(Lk\pi)^2]\tau}\right)$$

and $b=(u_0L_x)/a$, $C_1=L_y/(\lambda T_c)$, respectively. For this moving heat source, heat flux, q_0 and non-dimensional parameter, b are set at $q_0=1$ and $b=1$. The problem with time and space variable heat flux over a boundary is treated with by Beck et al. [14].

References

[1] C.K. Hsieh, K.C. Su, A methodology of predicting cavity geometry based on scanned surface temperature data – prescribed surface temperature at the cavity side, J. Heat Transfer 102 (2) (1980) 324–329.
[2] G.E. Bell, An inverse solution for the steady temperature field within a solidified layer, Int. J. Heat Mass Transfer 27 (12) (1984) 2331–2337.
[3] B. Lithouhi, J.V. Beck, Multinode unsteady surface element method with application to contact conductance problem, J. Heat Transfer 108 (2) (1986) 257–263.
[4] M. Shoji, N. Ono, Application of the boundary element to the inverse problem of heat conduction, Trans. JSME Ser. B 54 (506) (1988) 2893–2900 (in Japanese).
[5] C.H. Huang, C.C. Tsai, An inverse heat conduction problem of estimating boundary fluxes in an irregular domain with conjugate gradient method, Heat and Mass Transfer 34 (1998) 47–54.
[6] O.M. Alifanov, in: Inverse Heat Transfer Problems, Springer-Verlag, 1994, pp. 5–8.
[7] J.V. Beck, B. Blackwell, C.R. Clair, Inverse Heat Conduction, A Wiley–Interscience Publication, 1985.
[8] M. Imber, J. Khan, Prediction of transient temperature distributions with embedded thermo-couples, AIAA J. 10 (6) (1972) 784–789.
[9] M. Imber, Temperature extrapolation mechanism for two-dimensional heat flow, AIAA J. 12 (8) (1974) 1089–1093.
[10] M. Monde, Y. Mitsutake, Analytical method in inverse heat transfer problem using laplace transform technique, Int. J. Heat Mass Transfer 43 (21) (2000) 3965–3975.
[11] Monde et al., A new estimation method of thermal diffusivity using analytical inverse solution for one dimensional heat conduction, Int. J. Heat Mass Transfer 44 (16) (2001) 3169–3177.
[12] H.S. Carslaw, Conduction of heat in solids, second ed., Oxford University Press, 1959.
[13] R.V. Churchill, Fourier Series and Boundary Value Problems, McGraw-Hill, 1963.
[14] J.V. Beck, K.D. Cole, A. Haji-Sheikh, B. Litkouhi, Heat Conduction Using Green' Functions, Hemisphere Publishing Corporation, 1992.